EXPERIMENTAL GENERATION OF A DOUBLE-BUNCH ELECTRON BEAM BY TRANSVERSE-TO-LONGITUDINAL PHASE-SPACE EXCHANGE*

T. Maxwell[1,2,†], J. Ruan[2], P. Piot[1,2], A. Lumpkin[2], R. Thurman-Keup[2], A. Johnson[2], Y.-E Sun[2]
[1] Department of Physics, Northern Illinois University, DeKalb, IL 60115, USA
[2] Fermi National Accelerator Laboratory, Batavia, IL 60510, USA

Abstract

In this paper we demonstrate the generation of a tunable, longitudinal double-bunch electron beam. Experimental results on the generation of electron bunch trains with sub-picosecond structure have been previously reported where an initial transverse electron beam modulation was produced by masking the electron beam directly [1]. Here the initial transverse structure is imparted by masking of the photoinjector drive laser to effectively produce two horizontally offset beams at photoemission in the RF gun. A longitudinal double-bunch modulation is then realized after a transverse-to-longitudinal phase-space exchange beamline. Longitudinal profile tuning is demonstrated by upstream beam focusing in conjunction with downstream monitoring of single-shot electro-optic spectral decoding of coherent transition radiation.

INTRODUCTION

With the advent of transverse-to-longitudinal emittance exchange (EEX) [2, 3], mapping of the transverse distribution of an electron beam onto the current profile can be achieved. The feasibility of constructing uniform, linearly ramped, and high-frequency modulated current profiles by EEX of transverse beam modulations have been considered for the optimization of FEL, dielectric wakefield, and novel compact light source applications [4, 5].

Direct masking of the electron beam using transverse slits prior to EEX has been shown to produce a ps-scale density modulation with a corresponding enhancement of the coherent transition radiation (CTR) spectrum in the THz regime [1]. For photoinjector-driven systems, transverse masking of the drive-laser pulse can instead be used to impart the initial modulation providing some practical advantage. However, mapping of the laser profile to the accelerated transverse beam distribution is more indirect due to space charge and focusing in the RF gun [6]. Here we present a proof of principle, end-to-end measurement of the generation of a longitudinal double-bunch structure by laser masking.

APPARATUS

The A0 photoinjector (A0PI) facility [9] at Fermilab has provided electron beam in support of a variety of advanced accelerator R&D experiments over the last decade. Shown in Figure 1, the photoinjector utilizes a Cs_2Te photocathode located on the back plate of a 1-1/2 cell, 1.3-GHz, $TM_{010,\pi}$ mode RF gun. The photocathode is driven by the amplified, frequency-quadrupled output of a Nd:YLF drive laser. The system is capable of producing up to a 100-μs long train of pulses with a 1-MHz repetition rate and beam energy after the gun of 4 MeV. A 1.3-GHz, TM_{010}-mode, 9-cell superconducting RF (SCRF) booster cavity then provides acceleration up to 16 MeV.
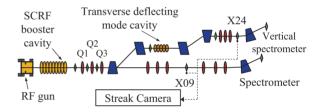

Figure 1: Top view of the A0 photoinjector. Optical paths from OTR stations X09 and X24 to the streak camera are shown. EOSD diagnostics are located at X24.

Masking of the drive laser is done in the laser lab prior to transport to the accelerator enclosure. The laser profile at the cathode is observed by virtual cathode image, a 1:1 image of the cathode plane. Transverse beam distribution after acceleration is deduced by standard beam imaging and slit techniques [10] after the booster cavity. Beam energy and energy spread are measured in the spectrometer at the end of the straight-ahead section with bunch length determined by imaging optical transition radiation (OTR) from an aluminized target in diagnostic cross X09 to an RF-synchronized streak camera.

A titanium-sapphire (Ti:sapph) laser system and electro-optic spectral decoding (EOSD) diagnostic system have recently been installed. The laser is a commercially available regenerative amplifier seeded by a 100-fs, 800-nm oscillator. A few-nJ, 5-ps chirped EOSD laser probe pulse is extracted from the amplifier synchronized to the first bunch in the electron bunch train.

EOSD of the CTR transient emitted from an aluminized target in cross X24 follows the standard configuration [7, 8] with slight modification. Light from X24 is imaged to a 1-
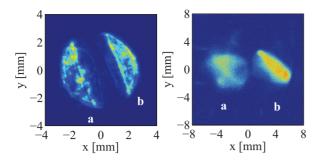
Figure 2: Raw images of the masked laser spot at the photocathode (left) and resulting transverse beam modulation after the SCRF booster cavity (right). Labels *a* and *b* are assigned to the two generated beamlets and their corresponding laser image regions.

mm thick ZnTe crystal with the linearly-polarized chirped laser pulse collinearly focused on the crystal. Decoding of the modulated laser pulse is accomplished by a circular polarizer followed by a polarization-resolving spectrometer. From this balanced EOSD detection scheme we deduce the sign-resolved CTR transient at the crystal. Further details on the laser commissioning and this EOSD setup are reported in [11, 12].

For perfect CTR imaging and uniform EOSD response, the decoded retardance $\Gamma(t)$ of the chirped laser spectrum is proportional to the transient of the CTR which is in turn proportional to the longitudinal charge distribution $\rho(t)$.

The thick-crystal response [13] and spectral decoding distortions [14] have been analyzed [12]. Effective temporal resolutions are found to be 0.5-ps and 1-ps FWHM. For imaging contributions, low-frequency diffraction losses are estimated to be significant when following the treatment of [15] with 50% attenuation at ~0.5 THz. For our configuration, strongest losses are due to the point-like sampling of the large, diffraction-limited CTR spot at the crystal over the spectrum of interest.

TRANSVERSE MODULATION

The drive laser mask is a 4-mm diameter aperture with a 1.5-mm wide rectangular block across the diameter. The virtual cathode image is shown in Figure 2. The magnification of the optical transport line from the laser room to the accelerator enclosure is observed with the image at the cathode having a hard-edge diameter of 6 mm. The two regions generated are labeled *a* and *b*.

Figure 2 also shows the resulting beam after the 9-cell accelerating cavity. The RF gun solenoid strengths are adjusted to produce a distinct transverse modulation. Precise imaging of the cathode image was not achieved. The laser mask is rotated to compensate for the corresponding change in the rotation imparted by Larmor precession [6]. Two distinct beamlets in *x* are resolved.

At 14.1 MeV the RMS bunch length σ_z after the booster cavity is 680-µm with momentum spread σ_p = 9.2 keV

Table 1: Results of transverse emittance measurement after acceleration for double beam shown in Figure 2, right.

Coord. u	x		y		
Beamlet	a	b	a	b	Units
$\langle u \rangle$	-3.43	3.43	0.01	-0.01	mm
$\langle u' \rangle$	-1.04	0.83	0.32	0.02	mrad
σ_{uu}	1.57	1.66	1.77	1.45	mm
$\sigma_{u'u'}$	0.10	0.08	0.13	0.10	mrad
$\sigma_{uu'}$	0.14	0.14	0.20	0.21	mm/mrad
ϵ_u^*	4.4	3.7	6.2	4.2	mm-mrad
$\epsilon_{u,\text{tot}}^*$	22		8.5		mm-mrad

for a normalized longitudinal emittance of 12.2 mm-mrad. Total bunch charge is q = 400 pC as measured by an integrating current transformer with q_a = 184 pC and q_b = 216 pC as computed from Figure 2. The transverse phase space ellipses of the beamlets were deduced independently with parameters summarized in Table 1. From Figure 2 we note that the full vertical extent is nearly identical in both cases (6 mm) while horizontally the beam is blown out to a width of ~12 mm. As demonstrated in [6], this can be explained by space-charge expansion in the low-energy regime during acceleration.

CONVERSION TO LONGITUDINAL MODULATION

Shearing of the transverse phase space prior to EEX is accomplished by upstream focusing. This in principle will map to a varied longitudinal profile after EEX. Quadrupoles upstream of the EEX line were set for currents of Q1 = 0.5 A, Q2 = -0.8 A, with Q3 varied around maximum beam compression (0.5 A). To see the effect of focusing and EEX, simulations were carried out using a MATLAB-based 3D ray-tracing program utilizing linearized transport matrices for machine parameters at A0PI. Gaussian beam populations with parameters from Table 1 are propagated from where the beam was measured to X24, where the EOSD is performed. Space charge effects are not included. The resulting longitudinal distributions at X24 as a function of the quad current Q3 are shown in Figure 3.

Figure 4 shows the measured transients from the decoded EOSD retardances as a function of quad current. As the diagnostic is sensitive to time of arrival, the image has been corrected for the 1-ps laser-to-beam jitter [12] by a row-shifting algorithm that temporally aligns neighboring shots based on the peak of their cross correlation.

Strong single-cycle oscillations are observed by EOSD in place of the Gaussian-like peaks expected of the current distribution. This has been analyzed and is consistent with the low-frequency filtering imposed by the previously mentioned THz imaging and sampling losses.

The FWHM microbunch durations Δt_i and their separation $\langle t_b \rangle - \langle t_a \rangle$ computed from Figures 3 and 4 are shown in Figure 5. Excellent agreement in the double-bunch spacing
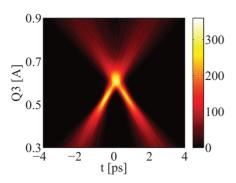
Figure 3: Simulated longitudinal distribution $\rho(t)$ as a function of the current applied to the final focusing quadrupole magnet Q3 before EEX.
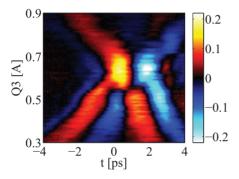

Figure 4: Decoded EOSD retardances $\Gamma(t)$ as a function of the current applied to the final focusing quadrupole magnet Q3 before EEX.

is observed. Discrepancies in the individual durations are likely due to a combination of measurement resolution and, more significantly, the linearized model used in simulation. Full simulations of A0PI by ASTRA and General Particle Tracker historically predict a minimum electron bunch duration of 1 ps in the presence of higher order and space-charge effects.
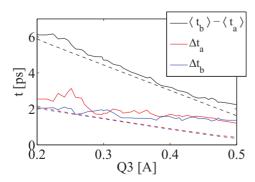

Figure 5: Measured (solid) and simulated (dashed) double-bunch spacings $\langle t_b \rangle - \langle t_a \rangle$ and FWHM durations Δt_i for the quadrupole scans shown in Figures 3 and 4.

DISCUSSION

A proof of principle, end-to-end measurement of the transfer of a transverse beam modulation imparted by drive-laser masking to the beam current profile after transverse-to-longitudinal emittance exchange has been carried out. The use of a laser mask provides practical advantages, though effects in the gun make precise beam imaging a challenge. Upstream focusing and a single-shot current profile diagnostic prove useful in live adjustments and beam dynamics studies. While more simulations of the measured distributions are forthcoming, the modulation is preserved to a readily measurable level for applications in intense pulsed THz or other compact light sources requiring multi-bunched electron beams.

ACKNOWLEDGMENT

REFERENCES

[1] Y.-E. Sun et al., Phys. Rev. Lett. **105**, 234801 (2010).

[2] J. Ruan et al., Phys. Rev. Lett. **106**, 244801 (2011).

[3] T. Koeth, Ph.D. thesis, Rutgers University, Piscataway, NJ (2009).

[4] P. Piot, Y.-E. Sun, J. G. Power, and M. Rihaoui, Phys. Rev. ST Accel. Beams **14**, 022801 (2011).

[5] W. Graves, F. Kaertner, D. Moncton, and P. Piot (2012), `arXiv:physics.acc-ph/1202.0318`.

[6] M. Rihaoui, P. Piot, J. G. Power, Z. Yusof, and W. Gai, Phys. Rev. ST Accel. Beams **12**, 124201 (2009).

[7] Z. Jiang and X.-C. Zhang, Appl. Phys. Lett. **72**, 1945 (1998).

[8] I. Wilke et al., Phys. Rev. Lett. **88**, 124801 (2002).

[9] J.-P. Carneiro et al., Phys. Rev. ST Accel. Beams **8**, 040101 (2005).

[10] M. Zhang, *Emittance formula for slits and pepper pot measurement*, FERMILAB-TM-1988 (1996).

[11] T. Maxwell, J. Ruan, P. Piot, and R. Thurman-Keup, in Proc. of IPAC2011 p. 1431 (2011).

[12] T. Maxwell, Ph.D. thesis, Northern Illinois University, DeKalb, IL (2012).

[13] B. R. Steffen, Ph.D. thesis, University of Hamburg (2007).

[14] J. Fletcher, Opt. Express **10**, 1425 (2002).

[15] S. Casalbuoni, B. Schmidt, and P. Schmüser, *Far-Infrared Transition and Diffraction Radiation*, TESLA Report 2005-15 (2005).